

Article

# Residual Stress Distribution and Microstructure Evolution of AA 6061-T6 Treated by Warm Laser Peening

Shu Huang<sup>1,2</sup>, Zuowei Wang<sup>1</sup>, Jie Sheng<sup>1,\*</sup>, Emmanuel Agyenim-Boateng<sup>1</sup>, Muxi Liu<sup>1</sup>, Xiaole Yang<sup>1</sup> and Jianzhong Zhou<sup>1</sup>

<sup>1</sup> School of Mechanical Engineering, Jiangsu University, Zhenjiang 212013, China; huangshu11@sina.com (S.H.); 18852861196@163.com (Z.W.); boatagenim@gmail.com (E.A.-B.); cooshine@163.com (M.L.); yxl93312138@163.com (X.Y.); zhoujz@ujs.edu.cn (J.Z.)

<sup>2</sup> School of Mechanical and Electrical Engineering, Xuzhou Institute of Technology, Xuzhou 221111, China

\* Correspondence: shengjie@ujs.edu.cn; Tel.: +86-511-8878-0219

Academic Editor: Patrice Peyre

Received: 12 September 2016; Accepted: 17 November 2016; Published: 22 November 2016

**Abstract:** The aim of this paper is to study the effects of laser peening (LP) on the residual stress distribution and microstructure evolution of AA 6061-T6 under different temperatures. A laser peening experiment was conducted on the square-shape samples by using single spot and 50% overlap shock. Three-dimensional surface morphologies of treated samples were observed. The influence of peening temperature on the distribution of compressive residual stress was analyzed. An optical microscope (OM) and a transmission electron microscope (TEM) were employed to observe the microstructure evolution of the samples before and after LP. The results indicate that, as the peening temperature increases, the micro-hardness increases first and then decreases. The LP process induces high-amplitude compressive residual stress on the surface at different temperatures even if the compressive residual stress slightly reduces with increases in temperature. The maximum compressive residual stress affected layer depth is about 0.67 mm, appearing at a temperature of 160 °C. The OM test revealed that the grain size was significantly decreased after warm laser peening (WLP) and that the average value of grain size was reduced by 50%. The TEM test shows that more dislocation tangles were produced in AA 6061-T6 after WLP; compared to the LP process, the precipitate-dislocation interaction can benefit both strength and ductility for AA 6061-T6, thus enhancing the mechanical properties of the material.

**Keywords:** AA 6061-T6; laser peening; temperature; surface integrity; microstructure

## 1. Introduction

AA 6061-T6 is an Al–Mg–Si–Cu alloy which is widely used in aerospace industry, ship manufacturing, and rail truck fields due to its high strength, good plasticity, and good performance in weldability and corrosion resistance. However, it has been found that micro cracks are likely to occur on the AA 6061-T6 surface at a specific strain rate and service temperature, resulting in fatigue failure [1]. Hence, the need to employ new technology to improve the mechanical properties, in particular the surface performance, and prolong the fatigue life of AA 6061-T6 alloy parts is worth the necessary attention.

LP utilizes a high-intensity laser pulse on the metal surface, which is covered by an absorbing layer (black tape or aluminum foil) and a confining layer (water or glass), respectively. A laser pulse passes through the confining layer and hits the target surface, which is immediately vaporized and forms the plasma. The resulting plasma is confined by the confining layer and generates an extremely high amplitude of pressure of several GPa. As the peak pressure exceeds the dynamic yield

strength of the material, the shock wave induces plastic deformation on the surface and generates compressive residual stress on the surface of the metal. The LP process can refine the grain size and thus improve the abrasion resistance, corrosion resistance, fatigue performance, and other mechanical properties [2]. Rubio-González et al. [3] found that LP-treated AA 6061-T6 specimens received an increment of 15% in fracture toughness compared with the untreated material. Such fatigue benefit is probably derived from the induced compressive residual stress by LP [4]. This conclusion is further verified by Irizalp's group [5]. Their research also revealed that the enlarged stacking fault ribbon, the new-formed deformation twins, and the increased twin boundary in the LP-treated AA 6061-T6 alloy may aid in the enhancement of both strength and high ductility [6]. Our research group has conducted many works that have focused on the effects of LP treatment on the fatigue behaviour of AA 6061-T6, including fracture morphologies [7], fatigue crack growth properties [8,9], and fracture microstructure evolution [10]. The results showed that LP is an effective surface treatment technique that can induce beneficial compressive residual stress and microstructures, such as a high density of dislocation, mechanical twins, and refined grains, which eventually retards fatigue crack growth. However, LP-induced beneficial effects on fatigue properties have shown to be released at high temperature and cycle loading, consequently limiting its application [11–13].

To solve this problem, Liao's group [14,15] proposed so-called warm laser peening (WLP) technology. They would pre-heat the treated specimens at a certain temperature first and meanwhile perform the LP process on the warmed specimens. WLP combines the advantages of LP and dynamic strain aging (DSA) and produces extremely higher dislocation density and better thermal stability due to the dislocations by pinning "Cottrell Clouds". Our previous research verified WLP as an effective process to maintain more stable compressive residual stress on the surface of a treated Ti-6Al-4V alloy, resulting in better fatigue performance [16]. From the micro aspect, Ye's group observed some nanoscale precipitates in the WLP-treated AA 6061-T6 [17], and it is preliminarily believed that these ultra-high-density nano-precipitates greatly improve the dislocation accumulation capacity and effectively increase the ductility of metals [18]. However, more convincing evidence and scientific data are required to validate the effectiveness of the WLP process on the surface properties.

In this work, the effects of LP temperatures on the micro morphologies and micro hardness were investigated. The residual stress was identified before and after the LP process at various temperatures, while the microstructures were also observed by the TEM method. The related strengthening mechanism of the WLP process on AA 6061-T6 was analyzed from both macro and micro aspects.

## 2. Materials and Experimental Procedure

### 2.1. Material and Specimen

AA 6061-T6 was selected in this work. Its chemical composition (wt. %) is as follows: 0.90Mg, 0.62Si, 0.33Fe, 0.28Cu, 0.17Cr, 0.06Mn, 0.02Ti, and 0.02Zn, and the rest is Al. The mechanical properties are as follows:  $\sigma_b = 356$  MPa,  $\sigma_{0.2} = 299$  MPa,  $\delta = 13.5\%$ ,  $E = 72.4$  GPa,  $\rho = 2672$  kg/m<sup>3</sup>, and  $\nu = 0.33$ .

Rectangular specimens with dimensions of 50 mm × 15 mm × 2 mm were employed. Both single spot peening and swept peening were conducted in the study, and the processing schematic is shown in Figure 1. All the specimens were polished by SiC papers with different grades (from 240# to 1000#), followed by ethanol ultrasonic cleaning before LP.

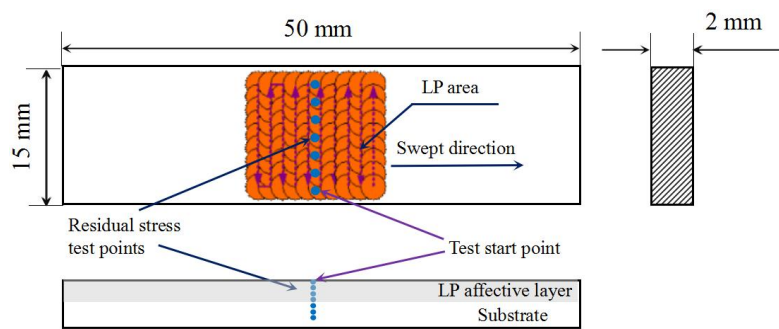


**Figure 1.** Dimension of specimen and treated area.

## 2.2. The WLP and LP Processes

WLP and LP treatment were both performed by a Q-switched Nd:YAG laser system operating at a 5 Hz repetition rate with a wavelength of 1064 nm and a pulse duration of 9 ns in fwhm. The spot diameter was 2 mm and the spot overlapping rate was 50%. The laser pulse energy used was 2 J. We utilized a self-developed heating device to achieve four different temperatures (25 °C, 100 °C, 130 °C, and 160 °C) for LP treatment. A special heat-resistant black adhesive tape was adopted as an absorbing layer, while the BK9 glass was used as the confining layer, as shown in Figure 2.

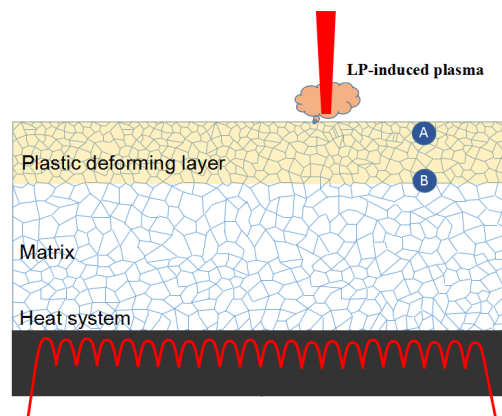


**Figure 2.** Set-up of warm laser peening.

## 2.3. Three-Dimensional Morphologies and Microstructure Observation

The single spot treated specimens were observed by Zeiss-Axio CSM 700 confocal microscopy (Carl Zeiss, Oberkochen, Germany). The influence of LP temperatures on the plastic deforming layer was analyzed from the three-dimensional morphologies. LEICA DFC420 optical microscopy (Leica, Solms, Germany) was used to study the grain size evolution in the treated region. The final microstructural details of LP-treated specimens were ascertained from TEM (JEM-2100, JEOL USA, Inc., Pleasanton, CA, USA) images at a voltage of 200 kV. For the TEM foil preparation, firstly, the sectioned specimen was grinded to a thickness of 150  $\mu\text{m}$  via two-side grinding. Then, the discs for TEM analysis were prepared by cutting ( $\phi 3$  mm), planar grinding (70  $\mu\text{m}$ ), and a final concave dimple grinding (20  $\mu\text{m}$ ). The final ion thinning was carried out via ion polishing (Gatan 691 PIPS, Gatan, Pleasanton, CA, USA) under an energy of 5 keV, and a small angle of incidence of nearly 4°.

## 2.4. Measurements of Compressive Residual Stress and Microhardness

In this study, compressive residual stress on the LP-treated surface and its in-depth were both detected by X-ray diffraction with the  $\sin^2\psi$  method. An X-ray tube with a chrome anode operated

at 20 kV was used. The X-ray beam diameter was about 1 mm. The X-ray source was a Cr-K $\alpha$  ray. The feed angle of the ladder scanning was 0.1° s<sup>-1</sup>. The scanning starting angle and terminating angle were 150° and 138°, respectively. Measurement points were selected on the surface with equal distance (0.5 mm) in the LP regions parallel to the laser swept direction as shown in Figure 1. An XF-1 electrolytic polishing machine (Shenzhen RPE Co., LTD, Shenzhen, China) was used to remove the material layer by layer. The residual stress value in-depth direction was detected on each layer. The microhardness of the treated surface at different temperatures was tested by a Vickers micro-hardness tester (HXD-1000TM, Shanghai Optical Instrument Factory, Shanghai, China) with a load of 200 gf and a holding time of 10 s.

### 3. Results and Discussion

#### 3.1. Effects of Temperature on Three-Dimensional Morphologies

The three-dimensional morphologies of LP-treated specimens at different temperatures are shown in Figure 3. LP-produced circle-shape dents are observed in all cases. The diameter of the plastic deforming dent is a little less than the laser spot. Due to the Gaussian distribution of the laser, the maximum deforming area locates in the spot center, and the deforming level gradually reduces away from the center region. From Figure 2, it can be seen that the depth of the single-spot-dent are 48.6  $\mu\text{m}$ , 58.8  $\mu\text{m}$ , 67.3  $\mu\text{m}$ , and 73.4  $\mu\text{m}$  at temperatures of 25 °C, 100 °C, 130 °C, and 160 °C, while the diameters are 1482.0  $\mu\text{m}$ , 1519.8  $\mu\text{m}$ , 1626.0  $\mu\text{m}$ , and 1711.1  $\mu\text{m}$ , respectively. This indicates that the diameter and the depth of the dents increase with an increment in LP temperature. We can infer that the thermal effect softened the AA 6061-T6, and the thermal-mechanical interaction induced by LP further aggravates the plastic deformation. In addition, as the temperature increases, the increment of dent depth and diameter reduces. For instance, the increment of the dent depth and the diameter are 14.5% and 7.0%, respectively, from 100 °C to 130 °C, while the values decrease to 9.0% and 5.2%, respectively, from 130 °C to 160 °C. This indicates that further deformation becomes harder even if temperature rises.

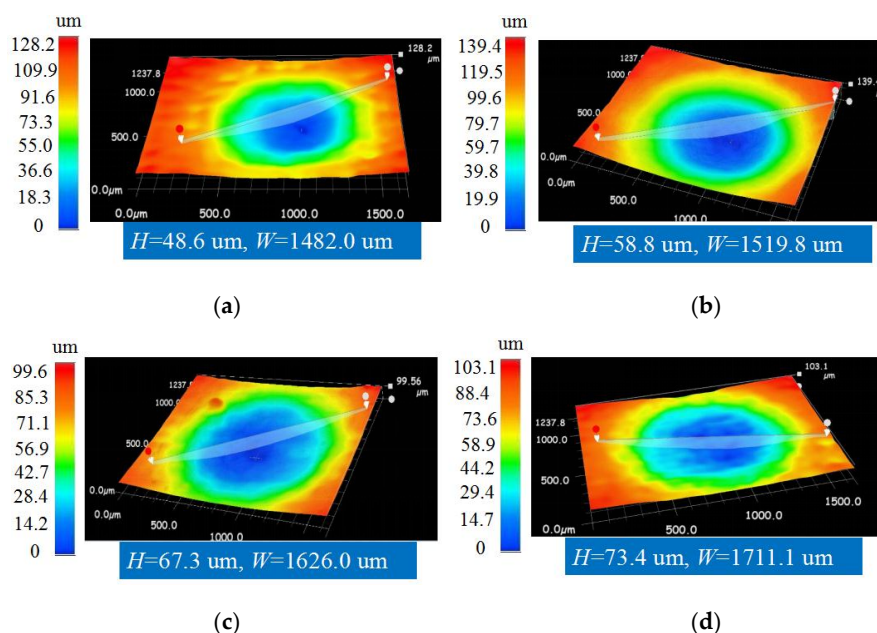


**Figure 3.** Three-dimensional morphologies of LP-induced dent at different temperatures: (a) LP at 25 °C; (b) WLP at 100 °C; (c) WLP at 130 °C; (d) WLP at 160 °C.

### 3.2. Residual Stress Distribution

The surface residual stress distribution at different temperatures is shown in Figure 4. It is noted that the compressive residual stress fluctuates with minor amplitude on the treated surface. The average compressive residual stress of specimens at the temperatures of 25 °C, 100 °C, 130 °C, and 160 °C are 232 MPa, 221 MPa, 207 MPa, and 200 MPa, respectively. When compared with 25 °C, the residual stresses are slightly decreased by 4.7%, 10.8%, and 13.8%, respectively at the temperatures of 100 °C, 130 °C, and 160 °C. This indicates that, in our study, the surface compressive residual stress induced by WLSP slightly decreases with increases in temperature.

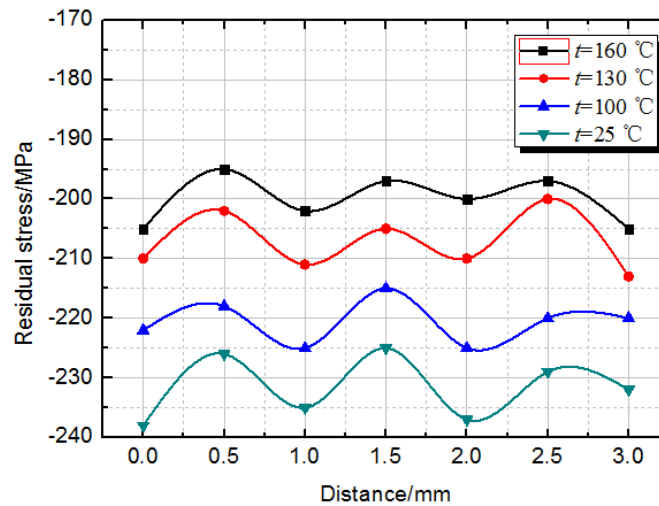


Figure 4. Surface residual stress distribution at different temperatures ( $P = 1.8 \text{ J}$ ).

The compressive residual stress induced by LP can be described by [19]

$$\begin{cases} \sigma_x = Ekp_{\max}e^{-bx/E} \\ \sigma_y = \frac{E\nu}{\nu-1}kp_{\max}e^{-bx/E} \\ p_{\max} = 0.01\sqrt{\frac{\alpha}{2\alpha+3}}\sqrt{ZI_0} \end{cases} \quad (1)$$

where  $E$  is elasticity modulus,  $k$  and  $b$  is constant,  $p_{\max}$  is peak pressure of laser shock,  $x$  is the depth along shock wave path,  $\alpha$  is 0.10–0.15,  $Z$  is acoustic impedance,  $I_0$  is laser power intensity, and  $\nu$  is Poisson’s ratio. When considering temperature  $T$ , we introduce an equation regarding  $T$  and  $E$  [20]:

$$E = E_0 (1 - 25k'T) \quad (2)$$

where  $E_0$  is the initial elasticity modulus, and  $k'$  is the thermal coefficient of expansion. Combining Equations (1) and (2), compressive residual stress can be obtained:

$$\begin{cases} \sigma_x = E_0 (1 - 25k'T) kp_{\max}e^{-bx/E_0(1-25k'T)} \\ \sigma_y = \frac{E_0(1-25k'T)\nu}{\nu-1}kp_{\max}e^{-bx/E_0(1-25k'T)} \end{cases} \quad (3)$$

From Equation (3), compressive residual stress  $\delta_x$ ,  $\delta_y$  are reduced by the increase in temperature. Juijerm’s study shows that, during the plastic deformation process of AA 5083, high temperature leads to a much lower magnitude of compressive residual stress compared with room temperature, which is consistent with our study [21]. However, Ye et al. claimed that WLP generates a higher magnitude of compressive residual stress than RT-LP for AA 7075 due to its effects on surface dislocation arrangement [18]. In fact, the generation mechanism of compressive residual stress on the aluminum alloy under high temperature is extremely complex. The interaction of plastic strain, stress recovery,

and thermal field results in the production of a final compressive residual stress. To sum up, which influence factor dominates varies in different material systems and processes. Obviously, the stress recovery dominates in our study.

Figure 5 shows the residual stress distribution in the depth direction at different temperatures.

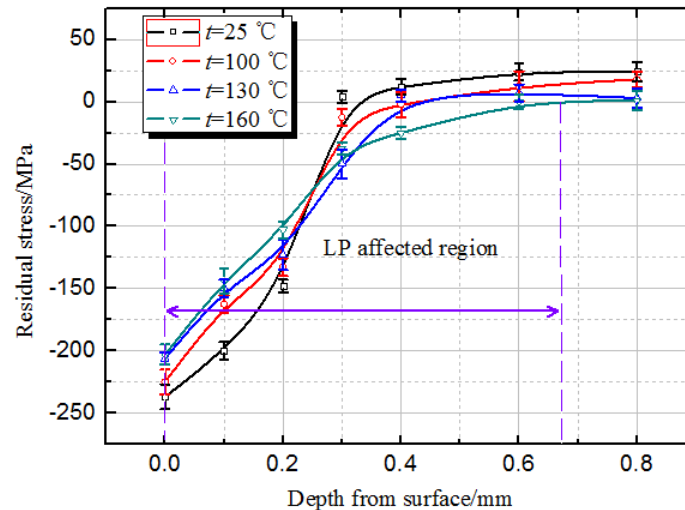
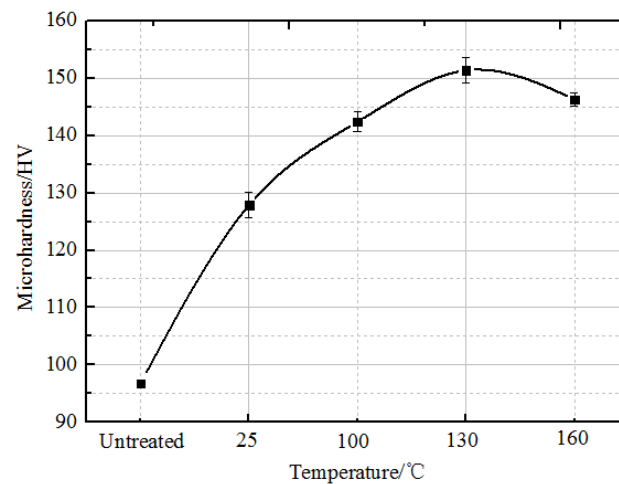


Figure 5. Residual stress distribution in the depth direction at different temperatures.

When we compare the magnitude of residual stress at the same depth, it can be found that, near the surface (0, 0.1, and 0.2 mm deep), LP-treated specimens with a lower temperature achieve a higher compressive residual stress. However, from the depth of 0.3 mm, the test point at a higher temperature achieves higher compressive residual stress. For instance, when a depth of 0.3 mm is achieved, the temperature of 130 °C achieves the highest value of  $-50$  MPa. Another interesting result is that the depth of the residual stress affected layer is 0.35 mm at 25 °C, while this value increases to 0.67 mm at 160 °C. Therefore, it can be concluded that, in this study, although the compressive residual stress slightly decreases with increases in LP temperature near the surface, the elevated temperature is still an effective factor that helps the LP process produce higher and deeper compressive residual stress in the depth direction, which may enhance the stress stability at a severe working condition. According to Nikitin's study, deeper residual stress is beneficial for inhibiting the initiation and propagation of fatigue crack, resulting in a longer fatigue life [22].

### 3.3. Microhardness

The LP experiment was carried out from 25 °C to 160 °C. As shown in Figure 6, material hardness increases gradually as temperature increases. The maximum hardness increased by 56.4%, appearing at the temperature of 130 °C. Furthermore, the WLP-treated specimens achieve higher microhardness compared with the LP process. This surface hardening phenomenon is attributed to both the strain hardening effect through the surface plastic deformation and the precipitation hardening effect through the generation of second phase nano-precipitates at an elevated temperature. However, there is a significant drop in hardness when the temperature reaches 130 °C. It can be concluded that 130 °C is the optimal temperature for the WLP of AA 6061-T6 from the perspective of precipitate strengthening. This is well consistent with Ye's conclusion [18]. It is concluded that, for a specific metal, an optimal temperature exists, if the WLP temperature exceeds the optimal one, the strengthening effect will decrease.



**Figure 6.** Microhardness distribution at different temperatures.

### 3.4. Microstructure

Figure 7a,b exhibits the surface microstructure of untreated and LP-treated AA 6061-T6 at 25 °C. Figure 7c,d shows the microstructure of a WLP-treated specimen at 130 °C in Area A and B in Figure 2 respectively.

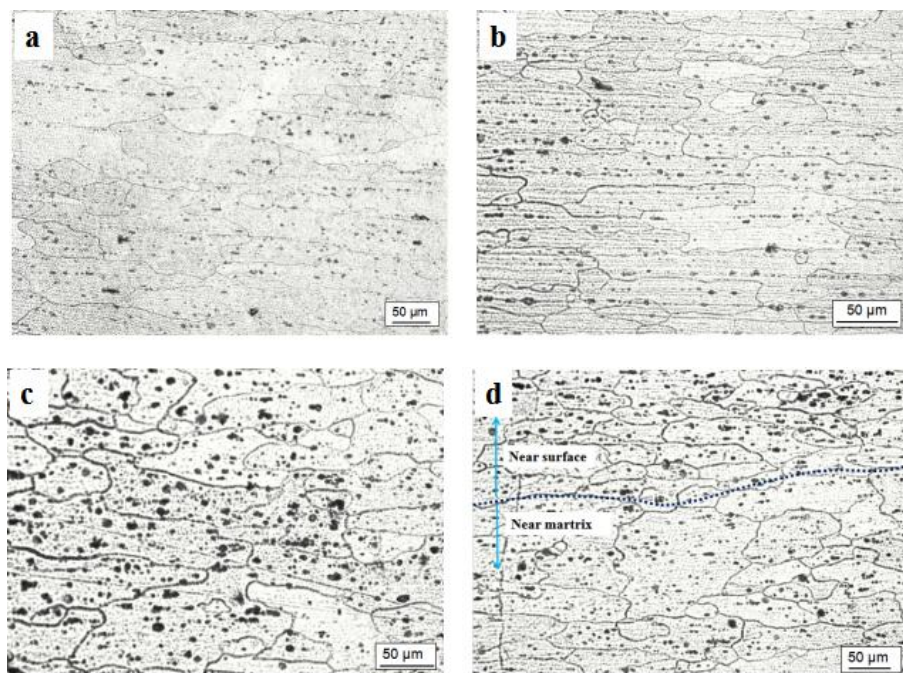


**Figure 7.** Microstructure: (a) untreated; (b) LP; (c) WLP in Area A; (d) WLP in Area B.

The grain size of the untreated sample (Figure 7a) is markedly larger than the treated samples (Figure 7b–d). The average size of the grains in Figure 6a is about 200  $\mu\text{m}$ , and this value decreases to 150  $\mu\text{m}$  and 100  $\mu\text{m}$  in Figure 7b,c. As we have discussed before, LP-induced dislocations are activated by the high temperature input and move freely. However, the high temperature promotes the phases precipitating, which block the movement of dislocations. As a result, the dislocation walls and cells are formed. At this time, edge dislocations gather at the cell walls, so the cell walls become thinner and clear sub-grain boundaries gradually form. Dislocation walls of polygonization

constitute small-angle sub-grain boundaries, dividing the original crystal into many sub-grains, and finally refine the grains [16]. Previous research has well proved that grain refinement induced by plastic strain in metals is of great help in enhancing surface properties. In particular, the compacted surface may inhibit the propagation of fatigue crack and thus enhance the fatigue life of service parts in some severe conditions [2–4]. However, the grain refinement will be weakened as the depth increases. In Figure 7c,d, an obvious boundary that divided the refining area and the matrix was found. This phenomenon complies well with the detection result of the compressive residual stress in depth. However, for the anti-fatigue research, we are more likely to concern the surface microstructure.

To further understand the strengthening mechanism of WLP, TEM morphologies are provided in Figure 8.

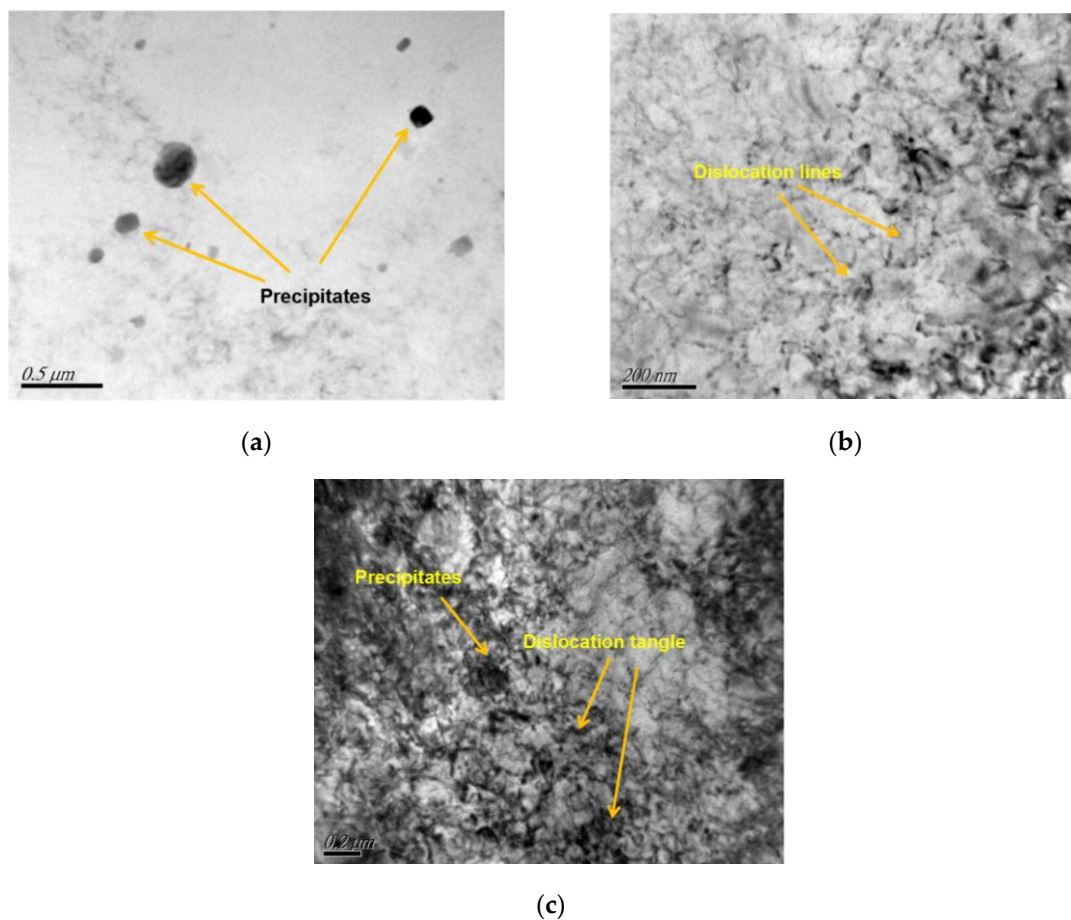


**Figure 8.** TEM images of the specimen at different temperatures for (a) before LP; (b) LP at 25 °C; (c) WLP at 130 °C.

It is noted that there is no dislocation distribution in the substrate (Figure 8a), but some precipitates are observed on the substrate surface, which may have been produced during the manufacturing process. By comparison, the LP/WLP-treated specimens exhibit plenty of dislocations, as can be seen in Figure 8b,c. In particular, a higher density of dislocations was observed when they were treated at high temperatures, as shown in Figure 8c. During the WLP process, many potential nucleation sites were formed near the new generated dislocations. On the other hand, at the DSA temperature, the solute atoms (Mg, Zn, etc.) have high mobility and efficiently diffuse and migrate to the dislocation cores. As a result, the solute atoms aggregate near the dislocation cores, which act as potential nucleation sites for the precipitates to grow, leading to more efficient dynamic precipitation. It is clear in Figure 8c that dislocations and precipitates are tangled with each other. The highly tangled precipitate–dislocation

interactions have relatively higher stability compared to dislocation structures without precipitates due to the beneficial pinning effect imposed by the precipitate particles. Ye's group employed HR-TEM to reveal that the precipitate particle is surrounded by high-density dislocations [18]. During plastic deformation, precipitate particles exert a pinning force to the dislocations nearby and thus increase the dislocation accumulation capacity. It is well known that high dislocation accumulation capacity is useful in enhancing material ductility. Hence, the precipitate-dislocation interaction can benefit both strength and ductility, this conclusion is also verified by Zhao [23] and Cheng [24]. To sum up, the WLP process induces more highly tangled strengthening phases and microstructures and makes a major contribution in terms of enhanced surface strength and improved residual stress stability.

#### 4. Conclusions

In this study, the effects of LP on AA6061-T6 surface integrity were investigated. Some important conclusions made are as follows:

- (1) LP induces high-magnitude compressive residual stress on the surface of a treated specimen at room and elevated temperatures even if the value of the stress slightly decreases with increases in temperature.
- (2) High temperatures assist LP in producing higher and deeper compressive residual stress in the depth direction, which may contribute to the stability of the induced residual stress and thus improve the component's life cycle.
- (3) LP at high temperatures was shown to have a significant effect on refining the grains' size, which may benefit the surface properties.
- (4) The precipitate-dislocation interaction during the WLP process may be a potential factor in improving the fatigue property of AA 6061-T6 parts under some severe service conditions.

**Acknowledgments:** The authors are grateful for the support provided by the National Natural Science Foundation of China (51405204 and 51575247), China Postdoctoral Science Foundation Funded Project (2014T70477 and 2013M540417), Jiangsu Planned Projects for Postdoctoral Research Funds (1401065B), and Advanced Talent Foundation of Jiangsu University of China (13JDG109), Opening Project of Jiangsu Key Laboratory of Large Engineering Equipment Detection and Control (JSKLEDC201503), Youth Key Teacher Training Project of Jiangsu University.

**Author Contributions:** Shu Huang and Jie Sheng conceived and designed the experiment; Zuowei Wang, Muxi Liu, and Xiaole Yang performed the experiments; Shu Huang analyzed the data and wrote the paper; Jiangzhong Zhou and Emmanuel Agyenim-Boateng revised the paper.

**Conflicts of Interest:** The authors declare no conflicts of interest.

#### References

1. Dorbane, A.; Ayoub, G.; Mansoor, B.; Hamadeb, R.; Kridlic, G.; Imadd, A. Observations of the mechanical response and evolution of damage of AA 6061-T6 under different strain rates and temperatures. *Mater. Sci. Eng. A* **2015**, *624*, 239–249. [[CrossRef](#)]
2. Lu, J.Z.; Luo, K.Y.; Zhang, Y.K.; Cui, C.Y.; Sun, G.F.; Zhou, J.Z.; Zhang, L.; You, J.; Chen, K.M.; Zhong, J.W. Grain refinement of LY2 aluminum alloy induced by ultra-high plastic strain during multiple laser shock processing impacts. *Acta Mater.* **2010**, *58*, 3984–3994. [[CrossRef](#)]
3. González, C.R.; Ocaña, J.L.; Rosas, G.G.; Molpeceres, C.; Paredes, M.; Banderas, A.; Porro, J.; Morales, M. Effect of laser shock processing on fatigue crack growth and fracture toughness of 6061-T6 aluminum alloy. *Mater. Sci. Eng. A* **2004**, *386*, 291–295. [[CrossRef](#)]
4. Rosas, G.G.; Gonzalez, C.R.; Ocaña, J.L.; Molpeceres, C.; Porro, J.A.; Morales, M.; Casillas, F.J. Laser shock processing of 6061-T6 Al alloy with 1064 nm and 532 nm wavelengths. *Appl. Surf. Sci.* **2010**, *256*, 5828–5831.
5. Irizalp, S.G.; Saklakoglu, N.; Akman, E.; Demirb, A. Pulsed Nd:YAG laser shock processing effects on mechanical properties of 6061-T6 alloy. *Opt. Laser Technol.* **2014**, *56*, 273–277. [[CrossRef](#)]
6. Gencalp, I.S.; Saklakoglu, N. High strength and high ductility behavior of 6061-T6 alloy after laser shock processing. *Opt. Lasers Eng.* **2016**, *77*, 183–190. [[CrossRef](#)]

7. Zhou, J.Z.; Huang, S.; Sheng, J.; Lu, J.Z.; Wang, C.D.; Chen, K.M.; Ruan, H.Y.; Chen, H.S. Effect of repeated impacts on mechanical properties and fatigue fracture morphologies of 6061-T6 aluminum subject to laser peening. *Mater. Sci. Eng. A* **2012**, *539*, 360–368. [[CrossRef](#)]
8. Huang, S.; Zhou, J.Z.; Sheng, J.; Lu, J.Z.; Sun, G.F.; Meng, X.K.; Zuo, L.D.; Ruan, H.Y.; Chen, H.S. Effects of laser energy on fatigue crack growth properties of 6061-T6 aluminum alloy subjected to multiple laser peening. *Eng. Fract. Mech.* **2013**, *99*, 87–100. [[CrossRef](#)]
9. Huang, S.; Zhou, J.Z.; Sheng, J.; Luo, K.Y.; Lu, J.Z.; Xu, Z.C.; Meng, X.K.; Dai, L.; Zuo, L.D.; Ruan, H.Y. Effects of laser peening with different coverage areas on fatigue crack growth properties of 6061-T6 aluminum alloy. *Int. J. Fatigue* **2013**, *47*, 292–299. [[CrossRef](#)]
10. Sheng, J.; Huang, S.; Zhou, J.Z.; Lu, J.Z.; Xu, S.Q.; Zhang, H.F. Effect of laser peening with different energies on fatigue fracture evolution of 6061-T6 aluminum alloy. *Opt. Laser Technol.* **2016**, *77*, 169–176. [[CrossRef](#)]
11. Altenberger, I.; Stach, E.A.; Liu, G.Y.; Nalla, R.K.; Ritchie, R.O. An in situ transmission electron microscope study of the thermal stability of near-surface microstructures induced by deep rolling and laser-shock peening. *Scr. Mater.* **2003**, *48*, 1593–1598. [[CrossRef](#)]
12. Zhou, Z.; Bhamare, S.; Ramakrishnan, G.; Mannava, S.R.; Langer, K.; Wen, Y.; Qian, D. Thermal relaxation of residual stress in laser shock peened Ti-6Al-4V alloy. *Surf. Coat. Technol.* **2012**, *206*, 4619–4627. [[CrossRef](#)]
13. Ren, X.D.; Zhan, Q.B.; Yuan, S.Q.; Zhou, J.Z.; Wang, Y.; Ren, N.F.; Sun, G.F.; Zheng, L.M.; Dai, F.Z.; Yang, H.M.; et al. A finite element analysis of thermal relaxation of residual stress in laser shock processing Ni-based alloy GH4169. *Mater. Des.* **2014**, *54*, 708–711. [[CrossRef](#)]
14. Liao, Y.L.; Ye, C.; Kim, B.J. Nucleation of highly dense nanoscale precipitates based on warm laser shock peening. *J. Appl. Phys.* **2010**, *108*, 063518. [[CrossRef](#)]
15. Ye, C.; Suslov, S.; Kim, B.J.; Stach, E.A.; Cheng, G.J. Fatigue performance improvement in AISI 4140 steel by dynamic strain aging and dynamic precipitation during warm laser shock peening. *Acta Mater.* **2011**, *59*, 1014–1025. [[CrossRef](#)]
16. Zhou, J.Z.; Meng, X.K.; Huang, S.; Sheng, J.; Lu, J.Z.; Yang, Z.R.; Su, C. Effects of warm laser peening at elevated temperature on the low-cycle fatigue behavior of Ti6Al4V alloy. *Mater. Sci. Eng. A* **2015**, *643*, 86–95. [[CrossRef](#)]
17. Ye, C.; Liao, Y.L.; Gary, J.; Cheng, G.J. Warm laser shock peening driven nanostructures and their effects on fatigue performance in aluminum alloy 6160 & dagger. *Adv. Eng. Mater.* **2010**, *12*, 291–297.
18. Ye, C.; Liao, Y.L.; Suslov, S.; Lin, D.; Cheng, G.J. Ultrahigh dense and gradient nano-precipitates generated by warm laser shock peening for combination of high strength and ductility. *Mater. Sci. Eng. A* **2014**, *609*, 195–203. [[CrossRef](#)]
19. Chen, R.F.; Hua, Y.Q.; Cai, L. Estimate of residual stress of steel materials induced by laser shock wave. *Chin. J. Lasers* **2006**, *33*, 278–282.
20. Wang, Y.G.; Chen, D.P.; He, H.L.; Wang, L.L.; Jing, F.Q. Temperature dependence of dynamic yield strength and spall strength for LY12 aluminum alloy under shock loading. *Acta Phys. Sin.* **2006**, *55*, 4202–4207.
21. Juijerm, P.; Altenberger, I. Effective boundary of deep-rolling treatment and its correlation with residual stress stability of Al-Mg-Mn and Al-Mg-Si-Cu alloys. *Scr. Mater.* **2007**, *56*, 745–748. [[CrossRef](#)]
22. Nikitin, I.; Altenberger, I. Comparison of the fatigue behavior and residual stress stability of laser-shock peened and deep rolled austenitic stainless steel AISI 304 in the temperature range 25–600 °C. *Mater. Sci. Eng. A* **2007**, *465*, 176–182. [[CrossRef](#)]
23. Zhao, Y.H.; Liao, X.Z.; Cheng, S.; Ma, E.; Zhu, Y.T. Simultaneously increasing the ductility and strength of nanostructured alloys. *Adv. Mater.* **2006**, *18*, 2280–2283. [[CrossRef](#)]
24. Cheng, S.; Zhao, Y.H.; Zhu, Y.T.; Ma, E. Optimizing the strength and ductility of fine structured 2024 Al alloy by nano-precipitation. *Acta Mater.* **2007**, *55*, 5822–5832. [[CrossRef](#)]

